

A mode-switching path planner for UAV-assisted search and rescue

by

Allison Ryan

B.S. (University of California, Berkeley) 2003

A dissertation submitted in partial satisfaction
of the requirements for the degree of

Master of Science

in

Mechanical Engineering

in the

GRADUATE DIVISION

of the

UNIVERSITY OF CALIFORNIA, BERKELEY

Committee in charge:

Professor J. Karl Hedrick, Chair
Professor Raja Sengupta

Spring 2005

Abstract

A mode-switching path planner for UAV-assisted search and rescue

by

Allison Ryan

Master of Science in Mechanical Engineering

University of California, Berkeley

Professor J. Karl Hedrick, Chair

Unmanned aerial vehicles (UAVs) can assist in U.S. Coast Guard maritime search and rescue missions by flying in formation with a human-piloted helicopter while using infrared cameras to search the water for targets. Current search and rescue flight patterns contain right-angle turns that can be achieved by a helicopter but not by a fixed wing UAV. Therefore, a necessity for UAV-assisted search and rescue is path planning and control that allows a UAV to track a helicopter performing such maneuvers while maintaining the desired sensor coverage and safety of all aircraft. A feasible path planning algorithm combined with an off the shelf autopilot system is proposed. Hardware in the loop simulations demonstrate satisfactory sensor coverage, but collision avoidance and tracking performance do not meet expectations.

Professor J. Karl Hedrick
Dissertation Committee Chair

Acknowledgements

I'd like to thank Professor Hedrick for supporting me in this research, and my lab mates in the Vehicle Dynamics Lab for their help and friendship. I'm especially grateful to Ryan Stauffer, for helping me work through the many challenges of this project, and to my parents.

Contents

1	Introduction	1
2	Problem formulation	4
2.1	Success metrics	4
2.2	Helicopter and formation assumptions	6
2.3	Solution framework	7
3	Solution: a set of four path rules	10
3.1	Cut Corner Path	10
3.2	Fixed Curve Path	11
3.3	Convergent Path	12
3.4	Outside Loop Path	13
3.5	Collision avoidance conditions	14
3.6	Convergence properties	16
4	Simulations	18
4.1	Search and Rescue aircraft and parameters	18
4.2	Simulation environments	21
4.3	Matlab convergence simulations	22
4.4	Hardware in the loop simulations	25
5	Conclusions and future work	31

Chapter 1

Introduction

The U.S. Coast Guard has expressed interest in the use of unmanned aerial vehicles (UAVs) to assist manned helicopters in maritime search and rescue missions. UAVs could increase the speed of a search using onboard infrared cameras, with no increased human risk, and at little additional cost. The search rate is increased by combining the helicopter's and UAVs' sensor footprints to form a larger contiguous footprint, and thereby searching more area. Increasing the search rate directly increases a victim's odds of survival, especially in cold water. In general, a search and rescue operation requires a trade-off between search speed and completeness, which will be further addressed in later sections. Briefly, a perfectly complete search may take an unacceptably long time (resulting in death by exposure), but a fast and incomplete search may never find the victim. A balance between these extremes is desired.

In the current U.S. Coast Guard (USCG) operating procedure, a search and rescue helicopter flies in a space-filling curve specified by the Coast Guard operating manual (2). Altitude, air speed, and pattern density are determined based on weather conditions, the visibility of the target, and other factors, all intended to ensure a reasonable probability of detection. When UAVs are introduced, the degree of overlap between the aircrafts' sensor footprints is another quantity to be balanced between search speed and completeness. A large overlap means that the UAVs improve the search rate less, but gaps between the

aircraft increase the probability of missing the target. The space-filling curve followed by the helicopter contains right-angle corners that are far more compatible with its own motion constraints than those of a fixed-wing UAV. Specifically, the helicopter is capable of decelerating, turning with a very small radius, and accelerating back to its cruising velocity. The UAV must fly at a relatively constant velocity and has a large turn radius. Thus, sensor coverage gaps are likely to occur at the corners of the helicopter's path.

The preference is to conduct UAV-assisted search and rescue with minimal modification of USCG hardware and procedures. Therefore, the hardware will consist of a number of UAVs, an unmodified Coast Guard helicopter, and the UAV central controller, to be located on the helicopter but not interfaced with onboard systems. The UAVs will have minimal onboard equipment, limited to a gimballed infrared camera and a waypoint-following autopilot. The camera is gimballed in order to counter the effects of the UAV's roll angle. The UAV's cruising speed will determine the nominal speed of the search pattern. The central controller will include a Global Positioning System receiver for Kalman filter estimation of the helicopter's location, velocity, and acceleration. It will also include the central controller (or groundstation) for the autopilot system, and a laptop computer to run the control. Due to lower communication requirements, the UAVs will be commanded by waypoints rather than turn rates. Given a feasible trajectory of waypoints, the autopilot will control the UAV's nonlinear dynamics, justifying the use of a kinematic model for the combined autopilot and UAV system, and the phrasing of the tracking control problem as path planning.

Because the aircrafts' altitudes are determined by target visibility and sensor specifications, altitude separation is not a favorable technique for collision avoidance. Instead, the UAV path planner will attempt to maintain safety by predicting the helicopter's trajectory and planning accordingly. It is preferable to incorporate collision avoidance directly into the path planner rather than using a general collision avoidance algorithm, because this way the collision avoidance's effects on ground coverage can be directly explicitly controlled and analyzed.

The path planner guarantees the safety of both aircraft under the assumption that the

helicopter continues to fly in the expanding square search and rescue pattern (described in section 2.2). In implementation, this must be combined with a lower level of collision avoidance that guarantees aircraft safety regardless of helicopter maneuvers. The general aircraft collision avoidance and evasion problem has been widely studied (8), and will not be addressed. Thus, this UAV-assisted search and rescue problem requires a two-dimensional path planning algorithm to produce safe, UAV-feasible 90-degree turns while maintaining the desired sensor coverage. In this project, a tracking controller specifically for a single UAV flying on the inside of an expanding square pattern will be developed.

Path planning in two dimensions for a vehicle with turn rate constraints is a well-studied problem, with much development based on Dubins' result (1). The search and rescue tracking problem differs from Dubins' result in that factors such as collision avoidance and ground coverage must be considered. Also, the goal is to track a moving rather than travel between fixed points. The adaptation of Dubins' result to tracking a moving target is addressed in (5), where a fixed point in the presence of constant wind is treated as a moving point in the wind-fixed frame. Previous work specific to UAV-assisted search and rescue addresses tracking of helicopter altitude changes and the effects of varying formation spacing on ground coverage and search speed (3).

Chapter 2

Problem formulation

The complete problem formulation includes success metrics, governing assumptions on the helicopter behavior and desired formation, and a proposed structure for the solution.

2.1 Success metrics

Search problems are characterized by a trade-off between search speed and completeness. A complete search guarantees that every target in the search area will be found. For stationary targets, this equates to applying a sensor to 100 percent of the search area. For moving targets, further assumptions must be made about the target's velocity and behavior (such as random motion or attempting to cross a border). In the case of search and rescue, the velocity of a drifting target will be much smaller than that of the aircraft, so it will be assumed that the target is stationary. Therefore, a complete search requires that the aircrafts' combined sensor footprint cover every part of the search area at least once. Search completeness will be measured as the percentage of the nominal search area that has been sensed.

Search speed measures the growth rate of the nominal searched area. For example, a helicopter may have a search rate of nine square miles per hour if it has searched a three by three mile region in that time, even if there were gaps in its sensor coverage. The UAV

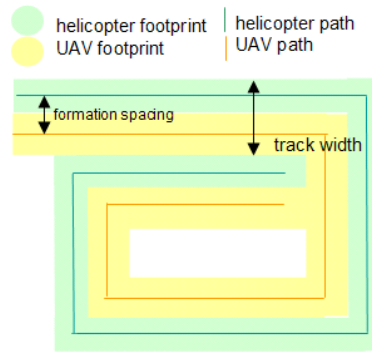


Figure 2.1. Definition of formation spacing and track width. These effect the search speed and completeness.

has a constant airspeed, so assuming the absence of wind, the search rate is determined by two factors: the track width of the space filling curve, and the formation spacing between the UAV and the helicopter. These are illustrated in figure 2.1. When the track width is equal to the width of the combined sensor footprint, there will be no gap in sensor coverage between adjacent tracks for the nominal trajectories shown. However, gaps still may occur at the corners of the path due to UAV tracking error. If the track width is further reduced, these gaps will be reduced, but the search speed with be decreased. It is assumed henceforth that the track width will be equal to the width of the combined sensor footprint. Thus, the search speed and completeness will depend only the the formation spacing and the effectiveness of the UAV in tracking the helicopter.

These metrics, completeness and search speed, can be used to prdict the likelihood of finding a target in a given time. A third metric, longitudinal tracking, has less direct effect on the search success, but reflects the UAVs ability to track the helicopter *along* its track. Because the UAV's airspeed is restricted to a small range, it is difficult to control its distance from the helicopter measured parallel to its velocity (longitudinally). Therefore, the path the UAV follows around a corner should have length such that the UAV and the helicopter are returned to their nominal formation when they rendezvous after the corner, rather than beginning the straight segment with a large longitudinal separation. The success of longitudinal tracking is measured as the aircraft turn a sequence of corners in the space filling curve.

2.2 Helicopter and formation assumptions

The helicopter will be modeled as following the expanding square spiral pattern as described in (2), which consists of straight segments (of increasing length) alternated with 90 degree right turns. Straight segments will be flown at constant velocity V , except when accelerating or decelerating for a turn. A turn is modeled as a constant deceleration from cruising velocity to zero velocity, an instantaneous turn, and a constant acceleration back to cruising velocity. Acceleration and deceleration have constant magnitude a . A Kalman filter (6) will be used to estimate both the current state (\hat{V}, \hat{a}) of the helicopter and the constant parameters of the spiral pattern (V, a) . Using these estimates, the helicopter observer predicts when the helicopter is about to make a turn so that the UAV can react accordingly.

When the helicopter is flying a straight segment, a nominal formation is defined in which the helicopter and the UAV are separated by a fixed distance d , perpendicular to their velocities. This distance is the formation spacing. In order to achieve a factor of redundancy f in the overlap of their sensor footprints, d must satisfy (2.1) where A is the aircrafts' altitude and β is the sensor field of view angle. This is shown in figure 2.2.

$$d = 2(1 - f)A \tan\left(\frac{\beta}{2}\right) \quad (2.1)$$

In the nominal formation, the UAV tracks a waypoint that is fixed relative to the helicopter at distance d . Therefore, when the helicopter turns a corner, the nominal formation results in an infeasible trajectory for the UAV. This means that the UAV's behavior will be unpredictable, and collisions are possible. This is the justification for the path planner which will be presented.

The UAV will be modeled with a limited turn rate and a constant velocity V equal to the helicopter's cruising speed. Because the search is conducted at a constant altitude and the autopilot controls the UAV's flight dynamics, only the yaw angle ψ will be modeled (a two-dimensional model). The turn rate limit will be interpreted as a minimum radius of curvature R for feasible UAV paths.

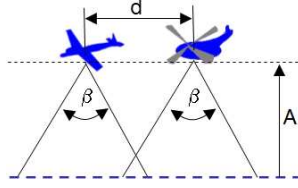


Figure 2.2. The distance between the helicopter's and UAV's parallel tracks is determined by their altitude (A) and angles of sensor coverage (β).

2.3 Solution framework

As explained previously, the search and rescue path planner is designed to enable a UAV to safely track a helicopter as it turns a series of right-angle corners. Thus, the search and rescue mission will be partitioned into straight segments and turn maneuvers. A straight segment is characterized by the aircraft maintaining fixed relative positions in the nominal formation described in the previous section. They also have constant airspeed. A turn maneuver occurs whenever the previous conditions are not met. Specifically, the turn maneuver begins at the instant that the helicopter begins to decelerate. At this instant, the UAV is located a distance L behind the helicopter, measured longitudinally as shown in fig. 2.3. The series $\{L(k)\}$ represents the distance by which the UAV lags behind the helicopter *at the start* of each of a series of turn maneuvers. For example, $L(1)$ is defined as the distance that the UAV lags behind the helicopter at the moment that the helicopter begins decelerating for the first corner. The turn maneuver ends when both aircraft have constant parallel velocities. A finish line can be fixed perpendicular to the aircrafts' new paths where they first become parallel, as shown in figure 2.3. The aircraft may reach this line at different times. Satisfactory longitudinal tracking could be characterized by the convergence of the series $\{L(k)\}$ to zero, or by bounding it by some acceptable values.

As previously mentioned, the helicopter and UAV have fixed relative positions during straight segments. Therefore, with the helicopter trajectory predetermined, the progression of $\{L(k)\}$ is determined only by the UAV's path during the series of turn maneuvers. The UAV will complete the turn maneuver in T_u seconds, and the helicopter in T_h seconds. Each time is measured from the beginning of the turn maneuver (when the helicopter begins to

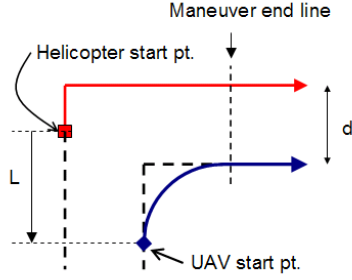


Figure 2.3. A representative turn maneuver showing UAV and helicopter positions at its start, and the finish line defined where their paths become parallel.

decelerate) to the time the individual vehicle arrives at the finish line. $L(k+1)$ can now be written as a function of T_u and T_h , where T_u will depend on $L(k)$ and the UAV's path during the turn maneuver. Any variation from a vehicle's expected route or velocity will appear as a disturbance, $\Delta(k)$.

$$L(k+1) = (T_u - T_h)V + \Delta(k) \quad (2.2)$$

The series $\{L(k)\}$ parameterizes the UAV's longitudinal tracking error through a series of turns, evaluating the continuous time tracking problem in terms of a single discretely evolving state. A control law's longitudinal tracking can now be easily evaluated based on the resulting convergence properties of $\{L(k)\}$. During the corner maneuver, the control law takes the form of a set of path planning rules, $\{R_i\}$, each of which is implemented when $L(k)$ falls within the associated domain, D_i . Implementation of path rule R_i results in a certain UAV path length, and corresponding time T_u . Therefore path rule R_i determines $L(k+1)$ based only on $L(k)$, by the progression function F_i associated with R_i as follows.

$$L(k+1) = F_i(L(k)) + \Delta \quad (2.3)$$

For any $L(k)$, $L(k+1)$ is determined by a particular path rule whose domain includes $L(k)$.

$$L(k+1) = \begin{cases} F_1(L(k)) + \Delta & L(k) \in D_1 \\ \vdots & \\ F_n(L(k)) + \Delta & L(k) \in D_n \end{cases} \quad (2.4)$$

The interaction of the set of path rules can be represented as a finite automaton with discrete states $\{R_i\}$ and invariants $\{D_i\}$. A transition from R_i to R_j is enabled when $L(k) \in D_i$ and $L(k+1) \in D_j$. A transition is made at each discrete time step, and because $\{D_i\}$ partitions the space of $L(k)$, exactly one will be enabled at each step and the execution will be deterministic in the absence of disturbance (7).

Chapter 3

Solution: a set of four path rules

The following four path planning rules form a solution to the search and rescue tracking problem. They guarantee convergence of $\{L(k)\}$ in spite of small disturbances, provide safe separation between the UAV and helicopter, and are formulated to provide contiguous ground coverage. The convergence property is based on a particular path rule (R_3) that always provides a path such that $L(k+1) = c L(k)$, where c is a convergence rate chosen between zero and one. The other path planning rules ensure that for any $L(1)$, $\{L(k)\}$ enters the domain of the convergent path rule in a small number of steps.

3.1 Cut Corner Path

For large values of $L(k)$, the UAV can safely "cut" the inside of the corner, resulting in $L(k+1)$ greatly reduced (fig. 3.1). The domain of R_1 is chosen such that this path rule applies when the UAV lags far behind the helicopter, but $L(k+1) \geq \min D_3$. D_3 is the domain of the convergent path rule. This prevents the existence of a cycle in the finite automaton.

$$\begin{aligned} D_1 &= \left\{ L(k) : L(k) > \frac{V^2}{2a} + 2d + \left(2 - \frac{\pi}{2}\right) R \right\} \\ F_1 &= L(k) - \frac{V^2}{a} - 2d + \left(\frac{\pi}{2} - 2\right) R \end{aligned} \quad (3.1)$$

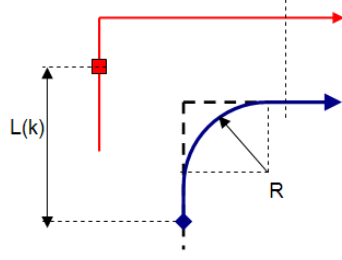


Figure 3.1. Cutting the corner (T_1) reduces large lag.

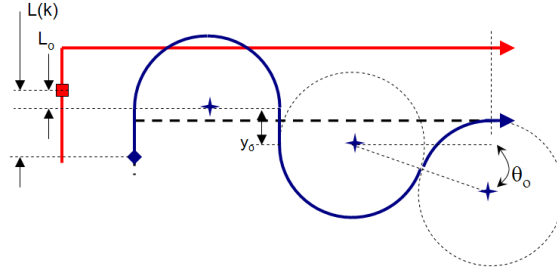


Figure 3.2. The fixed curve (T_2) causes constant reduction in lag and transitions smoothly to the convergent rule.

3.2 Fixed Curve Path

The fixed curve path rule (R_2) occurs on a domain in which the cut corner path rule would result in undesirably small $L(k + 1)$, but the convergent rule has inferior ground coverage properties. The minimum of D_2 is defined as $L(k) = L_0$. For $L(k) > L_0$, the fixed path rule is applied, and for $L(k) < L_0$, the convergent path rule is applied. The fixed path rule acts as a particular case of the convergent path rule, such that for $L(k) = L_0$, either path rule produces the same result, leading to a continuous progression between the two. As detailed in the following section, the convergent trajectory is a series of curves that has been designed to produce a desired path length. In this fixed trajectory, those curved sections are calculated according to the convergent trajectory rule for $L(k) = L_0$ (fig. 3.2). The fixed curve path rule then consists of a straight path from the UAV initial condition to that fixed set of curves. The fixed curve path keeps the UAV closer to its desired path than would implementing the convergent rule over their combined domains, $D_2 \cup D_3$.

$$\begin{aligned}
D_2 &= \left\{ L(k) : L_0 \leq L(k) \leq \frac{V^2}{2a} + 2d + \left(2 - \frac{\pi}{2}\right) R \right\} \\
F_2 &= (c-1)L_0 + L(k) \\
L_0 &= \frac{1}{c+1} \left[\left(\frac{5\pi}{2} - 4\right) R - \frac{2V^2}{a} \right] \\
c \in (0, 1) &\quad \text{chosen by designer in } T_3
\end{aligned} \tag{3.2}$$

3.3 Convergent Path

The convergent path consists of a half-circle, a straight segment, and two tangent arcs to lead the UAV back to its desired track. The angle θ decreases as the second arc is shifted farther from the UAV's desired track. This path rule is defined on a domain in which the UAV starts the turn on the near side of the helicopter's new path and angle θ (fig. 3.3) will be positive, i.e., the path consists of just one intermediate straight segment. $\theta(k)$ is a function of the length $y(k)$ of the straight segment, which is selected so that $\{L(k)\}$ converges geometrically to zero as in (3.3).

$$L(k+1) = c L(k), \quad c \in (0, 1) \tag{3.3}$$

$$\begin{aligned}
D_3 &= \\
&\left\{ L(k) : \frac{-V^2}{2a} < L(k) < \frac{1}{c+1} \left[\left(\frac{5\pi}{2} - 4\right) R - \frac{2V^2}{a} \right] \right\} \\
L(k+1) &= \\
&\left(\frac{5\pi}{2} - 2\theta(k) - 3 - 2\cos\theta(k)\right) R + y(k) - d - \frac{3V^2}{2a} \\
\theta(k) &= \arcsin\left(\frac{R+d-L(k)-y(k)-\frac{V^2}{2a}}{2R}\right)
\end{aligned} \tag{3.4}$$

$L(k+1)$ is a function of $\theta(k)$ and $y(k)$ such that it is not possible to solve explicitly for $y(k)$ based on the desired outcome (3.3). However, by fixing $L(k)$, $L(k+1)$ can be approximated very accurately as a linear function of $y(k)$ and replaced by its first order Taylor expansion. This can be used to solve for $y(k)$ in order to yield the desired $L(k+1)$. The linearization is calculated at y_o , which can be selected anywhere within an appropriate range because

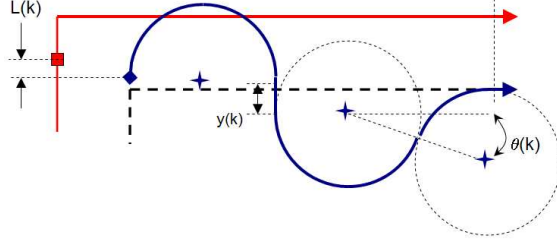


Figure 3.3. The convergent rule (T_3) causes $\{L(k)\}$ to converge exponentially to zero.

the function is approximately linear over the domain of interest.

$$\begin{aligned}
 L(k+1) &= f(L(k), y(k)) & (3.5) \\
 f(L(k), y(k)) &\approx f(L(k), y_o) + \left. \frac{\partial f}{\partial y} \right|_{y=y_o} (y - y_o) \\
 \left. \frac{\partial f}{\partial y} \right|_{y=y_o} &= 1 + \frac{1 - \sin \theta_o}{\sqrt{1 - \left(\frac{R+d-L(k) - \frac{V^2}{2a} - y_o}{2R} \right)^2}}
 \end{aligned}$$

The distance $y(k)$ can now be selected based on the approximation of its relation with $L(k+1)$.

$$y(k) = y_o + \frac{c L(k) - f(L(k), y_o)}{\left. \frac{\partial f}{\partial y} \right|_{y=y_o}} \quad (3.6)$$

3.4 Outside Loop Path

If the UAV begins the turn maneuver ahead of the helicopter's new path, as shown in fig. 3.4, its safe path is to loop back behind the helicopter. This will add significant length to the path, causing the UAV to lag behind the helicopter in the next turn.

$$\begin{aligned}
 D_4 &= \left\{ L(k) : L(k) < \frac{-V^2}{2a} \right\} \\
 L(k+1) &= \frac{3\pi}{2} R - \frac{3V^2}{2a} - d + \sqrt{R^2 + \left(L(k) + \frac{V^2}{2a} - d + R \right)^2} & (3.7)
 \end{aligned}$$

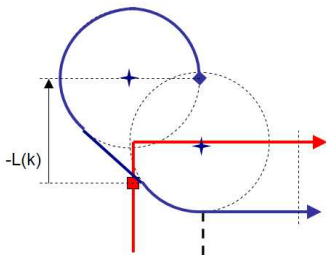


Figure 3.4. The outside loop path (T_4) greatly increases lag when UAV begins a turn ahead of helicopter.

3.5 Collision avoidance conditions

Collision avoidance will be addressed by the path planner rather than altitude separation because the optimal altitude is already set by the search conditions. In general, it is preferable that the UAV and helicopter paths do not intersect because this must preclude collisions. In the cases where they do intersect, safety can be ensured by showing that the aircraft do not pass through the intersection point at the same time. In this section, conditions will be derived to ensure collision avoidance in the absence of disturbances. The cut corner rule is not addressed because the helicopter and UAV do not cross paths. For the other rules, safety is conditional on the aircraft and formation parameters, velocity, acceleration, turn radius, and formation spacing.

In path rule two, the UAV begins its first arc at distance L_o behind the helicopter. If this distance is sufficiently large, the UAV will not cross the helicopter's path, and safety will be guaranteed. However, if the paths do cross, the aircraft may collide. The safety condition on L_o is the following.

$$L_o > R - \frac{V^2}{2a} \quad (3.8)$$

Substituting for L_o (3.2) leads to the following condition for the safety of this trajectory. Recall that c was chosen by the designer as the convergence rate of path rule 3, and note that the right hand side of 3.9 will always equal approximately 0.95.

$$\frac{V^2}{2aR} < \frac{\frac{5\pi}{2} - 5 - c}{3 - c} \quad (3.9)$$

Following path rule three, the UAV immediately begins turning in an arc that may

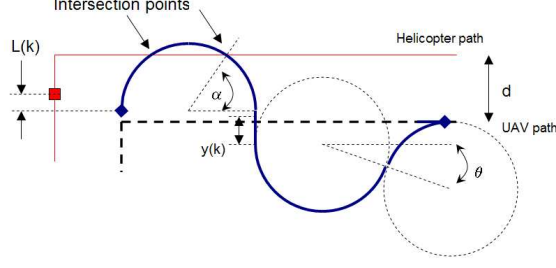


Figure 3.5. The two danger points for path rule 3, located at angles α and $\pi - \alpha$.

cross the helicopter's path twice, as shown in fig. 3.5. The intersection points are located at angles α and $\pi - \alpha$ along the arc. The UAV and helicopter pass through point one T_1 seconds apart and pass through point two T_2 apart. The worst case time differences for the vehicles passing through the two points are as follows.

$$\min T_1 = \frac{3V}{2a} + \frac{d+R}{V} + \frac{R}{V}(-\pi + \min_{0 \leq \alpha \leq \pi/2} \{\cos \alpha + \alpha\})$$

$$\min T_2 = \frac{3V}{2a} + \frac{d+R}{V} - \frac{R}{V} \max_{0 \leq \alpha \leq \pi/2} \{\cos \alpha + \alpha\}$$

The designer will likely specify some minimum clearance time T_d to ensure a factor of safety, resulting in the following requirement on V , a , and R .

$$\frac{3V}{2a} + \frac{d-R}{V} + \frac{R}{V}(3-\pi) > T_d \quad (3.10)$$

Although the UAV's and helicopter's paths intersect once in rule four, the helicopter passes through the intersection point almost immediately and the UAV passes through it only after completing a minimum turn radius loop. More specifically, the aircraft reach the intersection point at T_h and T_u respectively, and there will be no collision for the assumed range of parameters.

$$\begin{aligned} T_u &> 1.5\pi R/V \\ T_h &< \frac{V}{a} \end{aligned} \quad (3.11)$$

3.6 Convergence properties

Recall that $L(k)$ is the UAV's longitudinal tracking error at the beginning of the turn maneuver with index k in a series. We would like $\{L(k)\}$ to converge to approximately zero, resulting in perfect tracking. We show that this is true for any initial condition $L(1)$, and that the required number of corners for convergence is a bounded function of $L(1)$.

The convergence guarantee of the combination of path rules is based on the convergent rule (3.3), which causes $\{L(k)\}$ to approach zero as a geometric series. Thus, showing that all trajectories enter D_3 in finite time is equivalent to proving convergence for the system. Because in the absence of disturbances, $L(k+1)$ depends only on $L(k)$, the range $L(k+1) \in \mathfrak{R}_i$ of $L(k+1)$ for each path rule can easily be determined. Progression functions F_1 , F_2 , and F_3 are all linear and increasing in $L(k)$, and F_4 decreases monotonically with $L(k)$, resulting in the following.

$$\left. \begin{array}{l} \min \mathfrak{R}_i = F_i(\min D_i) \\ \max \mathfrak{R}_i = F_i(\max D_i) \end{array} \right\} i = 1, 2, 3 \quad (3.12)$$

$$\min \mathfrak{R}_4 = F_4(\max D_4)$$

Substituting the minimum and maximum of each path rule's domain into its progression function F_i produces the minimum and maximum of the range of $L(k+1)$ for each rule. Comparing these bounds to the domains of the path rules allows the possible transitions between path rules to be enumerated graphically as shown in figure 3.6. For example, the transition from rule 4 to rule 1 is enabled because there exists $L(k) \in D_4$ such that $F_4(L(k)) \in D_1$.

It can be seen from fig. 3.6 that the only loops in the transition graph occur from some domain back to itself, and that all paths either lead to the convergent domain or remain in a loop on T_1 or T_2 . Therefore, by showing that the loops on T_1 and T_2 can occur only a finite number of times, we show that $\{L(k)\}$ enters D_3 in finite time. This is easily shown by the fact that for both T_1 and T_2 , $L(k+1) = L(k) - C_i$, where C_i is a positive constant. D_1 and D_2 are both lower bounded, so the maximum number of executions (N_i) of either

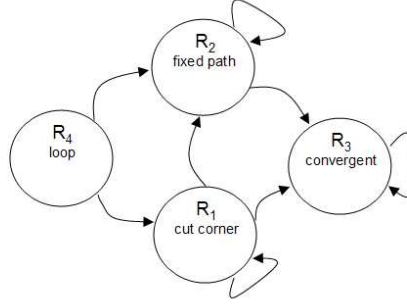


Figure 3.6. Possible transitions between domains of path rules

loop is bounded.

$$N_1 \leq (L(1) - \min D_1)/C_1 \quad (3.13)$$

$$N_2 \leq (\max D_2 - \min D_2)/C_2$$

Thus, for any initial condition, $\{L(k)\}$ reaches D_3 in $1 + N_1 + N_2$ steps or fewer, and then converges exponentially to zero in the absence of disturbance. When the UAV or helicopter deviates from its expected trajectory and introduces a disturbance, convergence can be ensured to a limited extent. Because the disturbance is not filtered through plant or controller dynamics, it cannot be attenuated. Therefore, a constant disturbance will result in steady state error. However, disturbances will not be amplified, and any single large disturbance has the same effect as restarting the system from an unfavorable initial condition, so convergence properties hold. A small random or periodic disturbance may slightly delay convergence, and after $\{L(k)\}$ enters the convergent domain, its variation will consist of the unfiltered disturbance.

Chapter 4

Simulations

4.1 Search and Rescue aircraft and parameters

For simulation, UAV physical parameters were taken from the SigRascal 110 airframe and experimental platform used by the Center for Collaborative Control of Unmanned Vehicles at the University of California, Berkeley (4). This is an off the shelf airframe that has been customized to carry a payload including a PC104 computer and a variety of cameras, as well as the Piccolo autopilot from CloudCap Technologies. The relevant parameters are the forward air speed (V) and the minimum turn radius (R). The air speed has been observed to range from 18 to 23 meters per second, but will be treated as constant at 20 meters per second. The minimum turn radius is approximately 100 meters. A helicopter used by the USCG for search and rescue operations is the HH-60 Jayhawk. Although it has a cruising speed of 72 meters per second, it will be restricted to match the UAV's cruising speed for simulation. It will also be assumed to have an acceleration (a) of 2.5 meters per second squared while following the expanding square pattern. The SigRascal UAV, Piccolo autopilot, and Jayhawk helicopter are shown in figures 4.1 - 4.3.

The nominal aircraft separation (d) is calculated as in 2.1 based on the search altitude (A) and the angle of the sensor field of view (β). The values given below do not include a factor of safety (overlap), which will be examined separately. A common field of view angle



Figure 4.1. SigRascal UAV airframe, with 2.8 meter wing span.



Figure 4.2. Piccolo autopilot system, from CloudCap Technologies. It is 12 cm long and weighs 90 grams.



Figure 4.3. HH-60 Jayhawk helicopter, approximately 20 meters in length.

for weather-proof infrared bullet cameras is 80 degrees. Search altitudes are given in (2) and depend on many factors including weather conditions and target size. For a human target, the suggested altitude ranges from 60 to 150 meters. For a small boat, the search altitude ranges from 300 to 900 meters. The search altitude should also be limited based on the requirement that the target occupy a desired number of pixels on the infrared camera CCD. The cameras examined provided images approximately 500 pixels across. It is desired that the target occupy at least 4 pixels. Thus, for a target of length s , the maximum allowable search altitude is as follows.

$$A = \frac{500s}{2 * 4 * \tan 40} \quad (4.1)$$

By this standard, a two-meter human requires a search altitude less than 150 meters, and a 20 meter boat requires a search altitude less than 1,500 meters. These conditions are satisfied by the altitude ranges suggested by the USCG manual. To summarize, the following parameters will be used for all simulations.

$$\begin{aligned}
V &= 20 \text{ m/s} \\
R &= 100 \text{ m} \\
a &= 2.5 \text{ m/s}^2 \\
A &= 150 \text{ or } 500\text{m} \\
\beta &= 80^\circ \\
d &= 250 \text{ or } 840\text{m}
\end{aligned}$$

Criteria for collision avoidance were given in section 3.5. Substituting the values above shows that the fixed path will be safe for any convergence rate chosen by the designer. In the convergent trajectory, the UAV will pass through the path intersection point more than 20 seconds before the helicopter for $d = 250$, and 50 seconds before the helicopter for $d = 840$. In the loop trajectory, the UAV will pass through the intersection point more than 15 seconds after the helicopter. Therefore, the set of parameters above is safe for all trajectories.

4.2 Simulation environments

The solution will be evaluated using two types of simulations: matlab simulations without UAV dynamics, and hardware in the loop simulations with full non-linear UAV dynamics. Matlab simulations assume that the helicopter executes the square spiral search pattern, and that the UAV perfectly tracks its assigned path. Therefore, the progression of $\{L(k)\}$ can be modeled as in (2.4) simply based on the lengths of each vehicle's path. Such simulations can be used to observe the ideal longitudinal tracking properties of the solution. However, these do not account for the dynamics of the UAV and autopilot, and do not result in simulated aircraft flight paths. Thus, they are less useful for evaluating safety or continuity of sensor coverage.

The hardware in the loop simulation capability of the Piccolo autopilot system combines the same autopilot used for flight testing with a six-degree of freedom non-linear aircraft

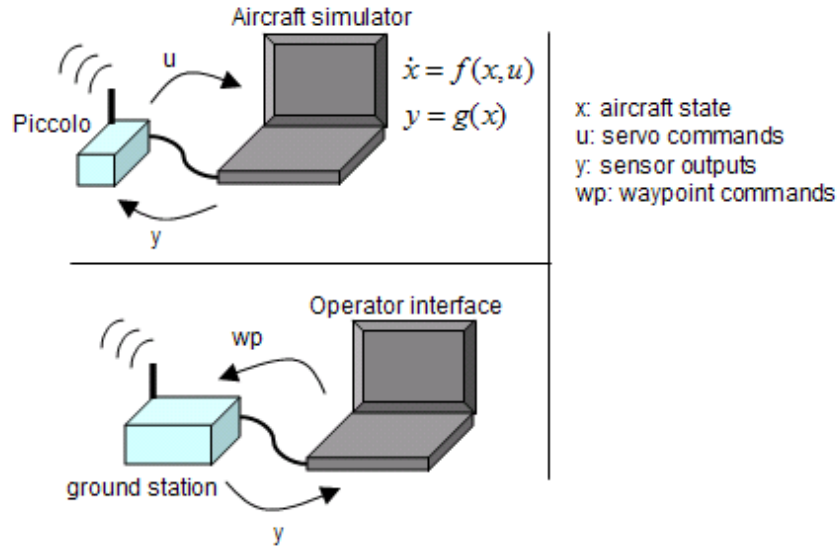


Figure 4.4. Schematic of hardware in the loop simulation.

model, resulting in high-fidelity simulations. As shown in figure 4.4, the Piccolo autopilot is connected to a laptop running a simulation of the aircraft model. This simulation reads the command outputs from the autopilot, interprets them as control surface deflections, and simulates the evolution of the aircraft state. Based on the state, such as altitude, airspeed, and turn rates, the simulator produces outputs for the Piccolo’s sensors, such as air pressure, GPS, and accelerometers. These simulated sensor outputs are used in the control loop by the autopilot, and are sent via wireless connection to the groundstation and operator interface. The resulting sensor coverage can be observed by plotting the aircrafts’ sensor footprints on top of their logged positions.

4.3 Matlab convergence simulations

Matlab simulations of the ideal system behavior can be used to predict the evolution of the UAV’s longitudinal tracking error through a sequence of corner maneuvers. Figure 4.5 shows the combined mapping from $L(k)$ to $L(k + 1)$ for the four path rules, which is the basis of these simulations. By noting the domains labeled on the vertical axis, one can infer the possible transitions from each domain. For example, the segment R_2 shows the range

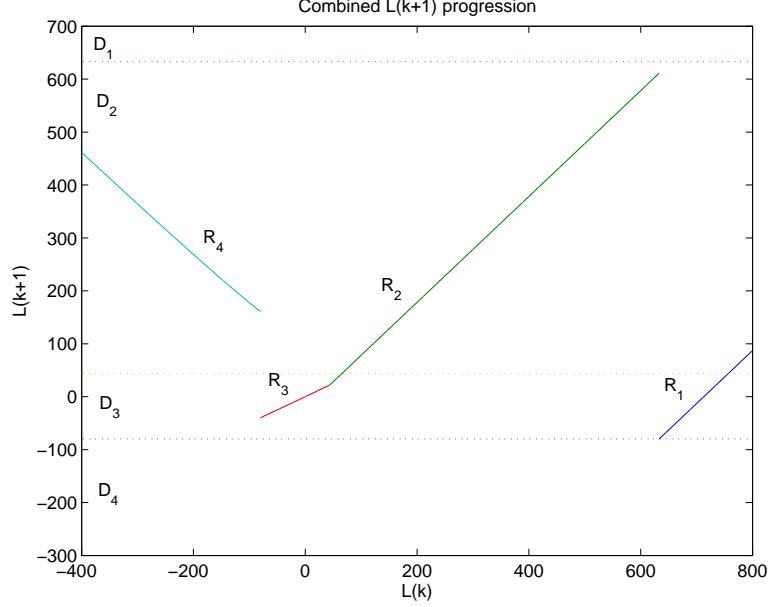


Figure 4.5. Combined mapping from $L(k)$ to $L(k+1)$ from all path rules. The horizontal lines show the boundaries between the path rule domains on the $L(k+1)$ axis.

of outcomes due to the fixed curve path rule. This segment exists in the second and third horizontal bands marked on the $L(k+1)$ axis, so R_2 can transition to R_2 and R_3 . The state transition diagram in figure 3.6 can also be inferred from this figure.

Figure 4.6 shows the progression of $\{L(k)\}$ in two simulations, one starting from an initial position 200 meters ahead of the helicopter, and the other starting 700 meters behind. In the first case, the UAV turns one corner using the loop rule, ten corners using the fixed curve rule, and then follows the convergent rule. In the second case, the UAV cuts the first corner and then immediately enters the convergent domain. Although the UAV's initial position is closer to the helicopter in the second case, it takes longer to reach its desired position because beginning ahead of the helicopter causes it to enter D_3 at an unfavorable position, requiring more corners before reaching the convergent domain.

Figure 4.7 shows the number of corners that the UAV must turn before arriving within 15 meters of its desired tracking position, over a range of initial conditions. Figure 4.8 shows an identical series of simulations, except with a random disturbance introduced between each turn maneuver. The disturbance is a random Gaussian variable with variance 10.

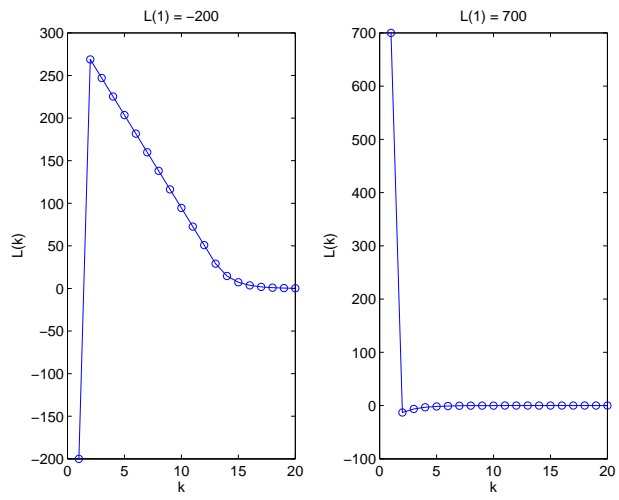


Figure 4.6. Simulated progressions of $\{L(k)\}$ starting from initial positions far behind (left) and ahead of (right) the helicopter.

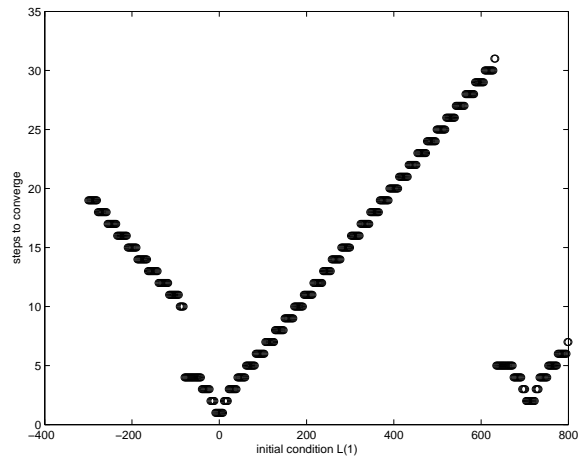


Figure 4.7. Number of corners before convergence over range of initial conditions. Convergence is defined as reducing tracking error to 15 meters.

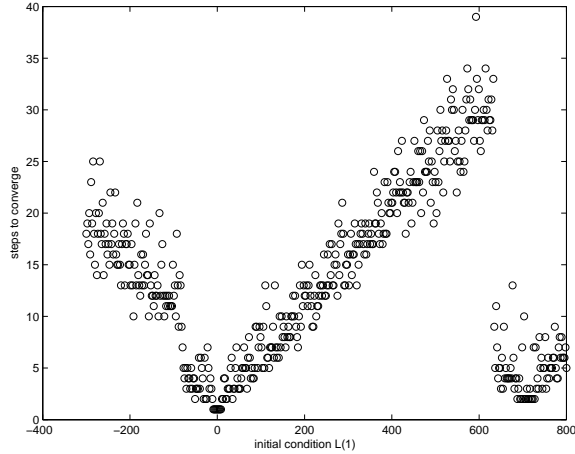


Figure 4.8. Number of corners before convergence, with Gaussian random disturbance of variance 10 at each corner. Convergence is defined as reducing tracking error to 15 meters.

4.4 Hardware in the loop simulations

Hardware in the loop simulations combine a high-fidelity UAV model with the actual autopilot and communications links that could be used for a flight test. The result is a log of each aircraft's simulated position recorded at approximately 1 Hz throughout the test. The helicopter's position comes from the kinematic model described in section 2.2, but the UAV's position comes from the interaction of the non-linear model, the autopilot, and the associated time delays for GPS reception and communication. Simulations run in real time, and require approximately an hour to complete. The main results of a simulation are the sensor coverage (percent of area covered), longitudinal tracking error sequence, and whether there were collisions between aircraft. The determining factors were altitude, formation spacing, and the effect of the mode-switching controller. The search altitudes for a human and a small boat (150 m and 500 m) were tested, with either the mode-switching controller, or with a waypoint fixed relative to the helicopter. At the lower altitude, formation spacings

with 0, 5, and 10 percent sensor overlap were tested.

<i>Test</i>	<i>Altitude</i>	<i>Mode switching</i>	<i>%overlap</i>	<i>%coverage</i>	<i>#collisions</i>
1	150	<i>yes</i>	0	99.65	0
2	150	<i>no</i>	0	99.51	0
3	150	<i>yes</i>	5	99.62	2
4	150	<i>no</i>	5	99.51	1
5	150	<i>yes</i>	10	99.82	2
6	150	<i>no</i>	10	99.78	0
7	500	<i>yes</i>	5	100.00	1
8	500	<i>no</i>	5	99.91	0

The percent sensor coverage is calculated using a 3 step process. First, paths of the aircraft are plotted (fig. 4.9). Then a sensor footprint of the appropriate diameter D is plotted at each data point according to the sensor geometry.

$$D = 2 * Alt * \tan\left(\frac{\beta}{2}\right) \quad (4.2)$$

The resulting plot is saved as an image and cropped to show only the area searched (fig. 4.10). An image processing tool is used to count the black and white pixels, resulting in the coverage percentage.

The test shown in figures 4.9 and 4.10 is test number one in the table above. Although there is no overlap in the sensor footprints, the coverage is still fairly good. Figure 4.11 shows a test (number two in table) under the same conditions, but with a fixed waypoint instead of the mode-switching controller. It can be seen that coverage gaps are larger and more frequent.

The six tests conducted at 150 meters altitude compare the sensor coverage of the mode-switching and fixed-waypoint controllers at a variety of formation spacings. Recall that the the search speed is inversely proportional to the degree of sensor overlap, so a larger overlap corresponds to a slower search. These results are shown in figure 4.12. As expected, the coverage tends to increase with sensor overlap, and the mode-switching controller performs better than the fixed-waypoint controller. However, the range of data is extremely small,

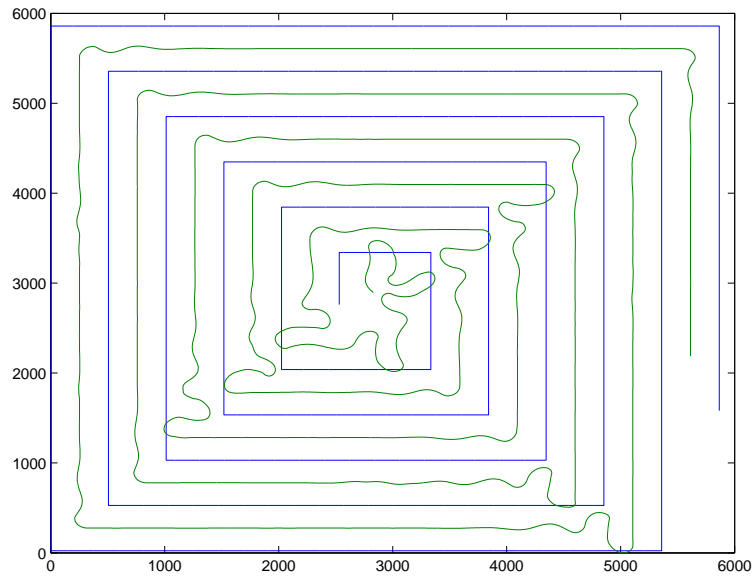


Figure 4.9. Aircraft paths from hardware in the loop simulation at 150 m altitude with no overlap in sensors. The mode-switching controller is used.

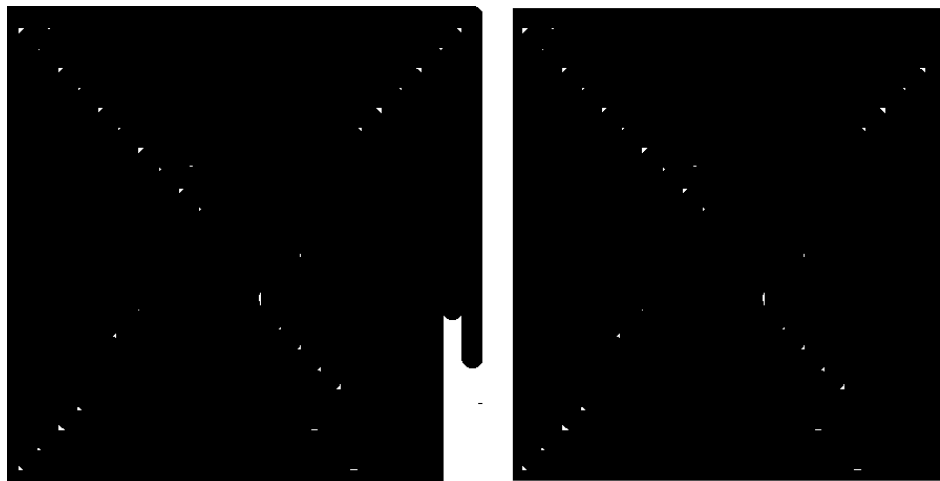


Figure 4.10. Bitmap image showing searched areas in black. Image on left shows entire test. Image on right is cropped to show largest nominally searched rectangle, and used for coverage calculation

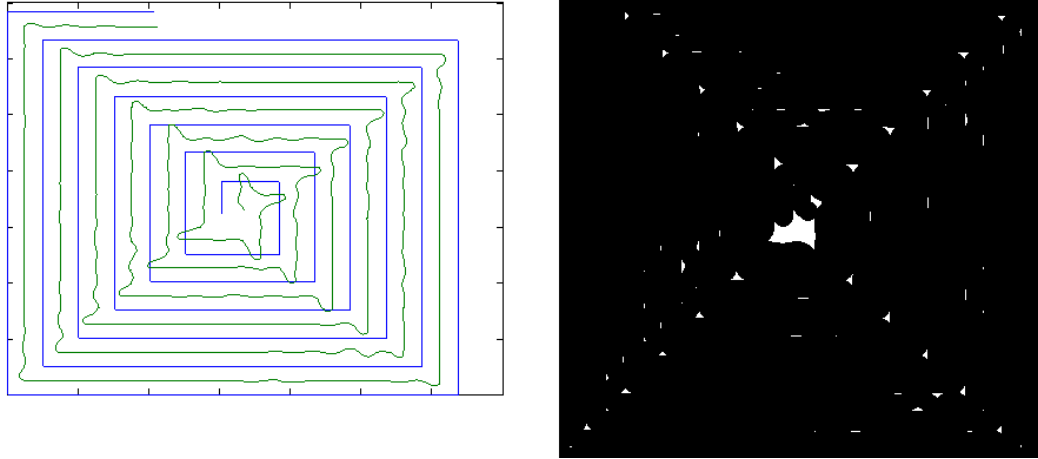


Figure 4.11. Test at 150 m altitude with 0 % overlap and waypoint fixed relative to helicopter.

with the results from all eight tests falling within a range of one half percent. At this scale, very small changes in initial conditions or image cropping may dominate the results. Therefore, although one can conclude that the mode-switching controller provides very good sensor coverage, there remains some doubt as to how it compares to the fixed-waypoint controller.

Although the mode-switching controller provides satisfactory sensor coverage, it does not display the predicted success in reducing tracking error between the UAV and the helicopter. In theory, the longitudinal tracking error ($\{L(k)\}$) should converge to near zero in fewer than 20 steps for all tests as shown in section 3.6. However, this behavior was never observed. In all tests, the mode-switching controller caused $L(k)$ to fluctuate over a large range, as shown in figure 4.13. Although the tracking error does not converge as desired, it does appear to be bounded rather than increasing. In contrast, the tracking error observed due to the fixed-waypoint controller is smaller, but increases linearly with k in all tests. A representative example is shown in figure 4.14. This suggests that for sufficiently long tests, the mode-switching controller may still provide better tracking.

It is desired that the path planner incorporate collision avoidance because an independent lower-level collision avoidance control could interfere with the desired ground coverage and convergence properties. Although section 3.5 showed that the UAV and helicopter

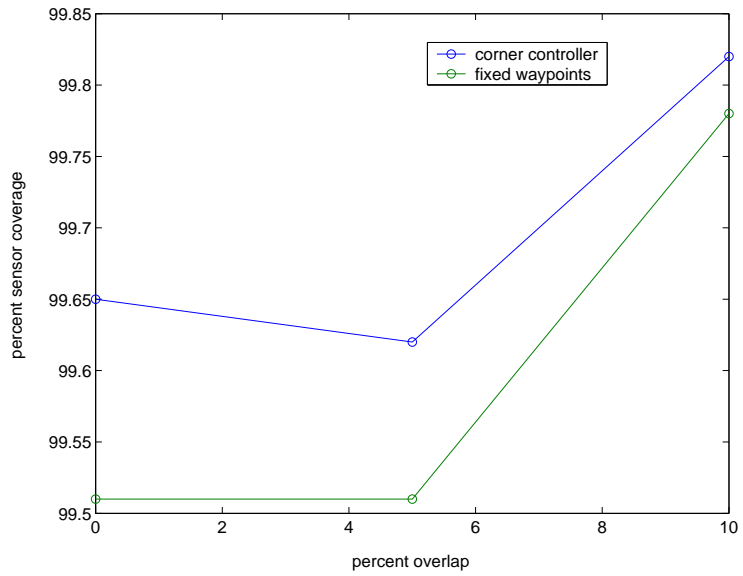


Figure 4.12. Sensor coverage due to mode-switching and fixed-waypoint controllers, at varying overlap in sensor footprints. A larger sensor overlap implies a slower search speed.

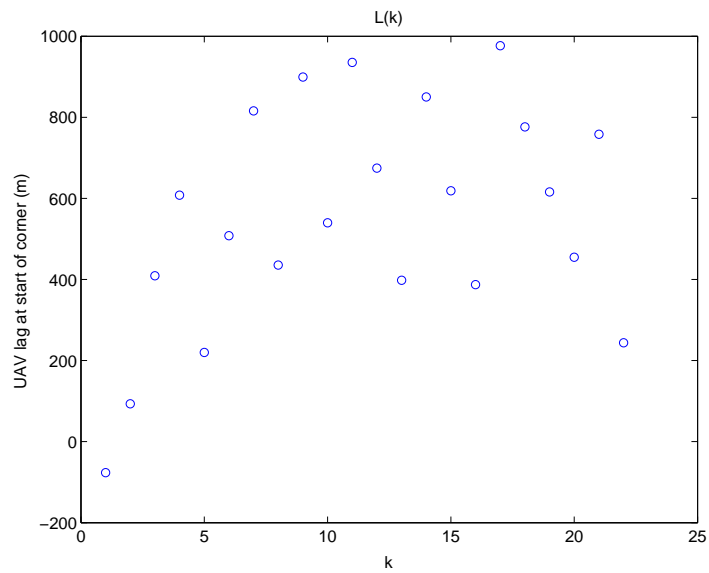


Figure 4.13. $L(k)$ fluctuates over a large range, instead of converging to zero as predicted. The test shown uses the mode-switching controller at altitude 150 meters, with 10 % sensor overlap.

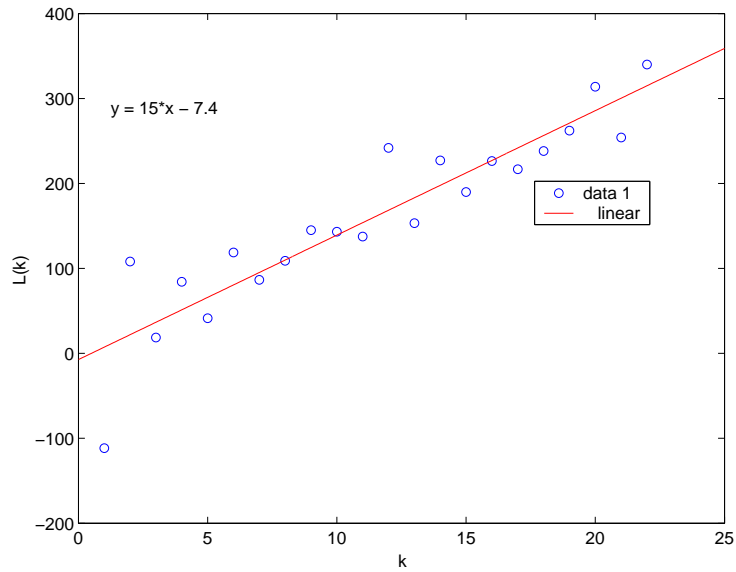


Figure 4.14. $L(k)$ increases linearly with the number of corners (k) when the fixed-waypoint control is applied. This test is at 150 meters altitude with 5 % sensor overlap.

should not collide under the conditions tested, this was not supported by hardware in the loop simulations. The mode-switching controller allowed, on average, 1.25 collisions per one-hour test. The fixed-waypoint controller, with no collision avoidance incorporated, produced on average 0.25 collisions per one-hour test. Thus, the mode-switching controller provided less safety than one that did not address collision avoidance.

Chapter 5

Conclusions and future work

A set of metrics was defined in section 2.1 to assess the success of a solution for the search and rescue problem. These were search speed, sensor coverage, and longitudinal tracking. In addition, collision avoidance was stated as a requirement. Based on the results of hardware in the loop simulations, the mode-switching path planner provides satisfactory search speed and coverage, as shown by the fact that near-complete sensor coverage can be provided without requiring excessive sensor overlap. However, the longitudinal tracking performance falls far below expectation, and the collision avoidance requirement was not met. This is because the system is not sufficiently robust to trajectory tracing error.

The fact that sensor coverage was satisfactory while longitudinal tracking performance and collision avoidance were not can be explained by their dependencies on quality of trajectory tracking. Sensor coverage is determined by the diameter of the sensor footprints on the ground. Small deviations from the UAV's assigned trajectory result in corresponding small movements of the sensor footprint from its nominal location, and deviations from the expected heading angle have no effect. However, longitudinal tracking performance and collision avoidance are based on expectations of the UAV's path length throughout a turn maneuver. Because the UAV has a large turn radius, small deviations in heading angle or position at the beginning of a turn maneuver can result in large deviations in path length, and therefore completion time. Because the tracking and collision avoidance properties

of the system are based on controlling turn maneuver completion time, they are strongly affected.

Deviations from expected trajectory and heading angle can be caused by a number of factors. Such deviations can be observed by comparing the ideal trajectories shown in section 3 with the trajectories produced by hardware in the loop simulation in section 4.4. Communication between the aircraft and the controller occurs at 1 Hertz, limited by the rate of the GPS signal used to determine the aircrafts' positions. Therefore, the Kalman filter estimation that detects the helicopter's deceleration and activates the mode-switching controller is delayed. This estimation is very important in predicting the UAV's future desired location. Also, the UAV's position data may be one second out of date when the control is calculated, and another second may pass before the control is sent. At the UAV velocity of 20 meters per second, the UAV travels 40 meters in two seconds. The characteristic scale of the desired maneuvers is the UAV's minimum turn radius, (100 meters) so the possible uncertainty of 40 meters due to time delay is likely to have a large affect.

In addition to time delay, tracking error can also be caused by the UAV's unmodeled non-linear dynamics, wind disturbances, and the effectiveness of the waypoint controller. As a result, trajectory tracking error will still be present even with increased communication rate. Therefore, a solution must be developed which is robust to vehicle position estimation uncertainty and tracking error.

The search and rescue controller developed here is a path planner that theoretically satisfies the stated goals of search completeness, speed, tracking error convergence, and collision avoidance. This is achieved using a mode-switching path planner that controls the UAV's path length in order to produce the desired longitudinal tracking. The path shape is formulated to provide sensor coverage on the ground, and a set of conditions is established in order to guarantee collision avoidance. These conditions are satisfied by the vehicle and mission parameters. Through hardware in the loop simulations, it is observed that the longitudinal tracking and collision avoidance properties are not robust to the observed errors in UAV trajectory tracking and aircraft position estimation. Therefore, although

the solution presented is theoretically acceptable, it is not sufficiently robust for real-world implementation.

Future work should begin with a more robust tracking algorithm for multiple UAVs, possibly based on turn rate rather way point control. This will allow tracking to be considered more directly as a control problem rather than path planning. Due to the requirement of a perfect safety guarantee for the manned helicopter, it should be assigned a different altitude than the UAVs. Thus the collision avoidance problem will be restricted to UAVs and not need to account for an unpredictable human pilot. For search and rescue implementation, behaviors such as formation reconfiguration, target detection and tracking must also be included.

Bibliography

- [1] L.E. Dubins, "On Curves of minimal length with a constraint on average curvature and with prescribed initial and terminal positions and tangents", *American Journal of Mathematics*. 79:497-516. 1976
- [2] *U.S. Coast Guard Addendum to the United States National SAR Supplement (CGADD)*, COMDTINST M16130.2C, Chapter 3 and Appendix H, available at: <http://www.uscg.mil/hq/g-o/g-opr/manuals.htm>
- [3] Anna Williams, *Search and rescue augmentation using unmanned aircraft*, Masters Thesis, UC Berkeley, 2004.
- [4] A. Ryan, M. Zennaro, A.S. Howell, R. Sengupta, and J.K. Hedrick, "An Overview of Emerging Results in Cooperative UAV Control", *Proceedings of the IEEE Conference on Decision and Control*, Dec. 2004.
- [5] T. McGee, S. Spry, and J.K. Hedrick, "Optimal path planning for an aircraft with a bounded turn rate in the presence of a constant wind", submitted to the *AIAA Conference on Guidance, Navigation, and Control*, August 2005.
- [6] R.E. Kalman, "A new approach to linear filtering and prediction problems", *Trans. of the ASME Journal of Basic Engineering*, Vol. 82, 1960.
- [7] John Lygeros, *Lecture notes on hybrid systems*, Feb. 2004.
- [8] Kuchar, J. K. and L. C. Yang, "A Review of Conflict Detection and Resolution Modeling Methods", *IEEE Transactions on Intelligent Transportation Systems*, Vol. 1, No. 4, 2000.